Review of Scientific Instruments

RESEARCH ARTICLE | JANUARY 24 2020

# Design and development of an Allison type emittance scanner for the SPIDER ion source

**Special Collection:** Proceedings of the 18th International Conference on Ion Sources

Carlo Poggi ; Emanuele Sartori; Marco Tollin; Matteo Brombin ; Matteo Zaupa ; Enrico Fagotti; Gianluigi Serianni



*Rev. Sci. Instrum.* 91, 013328 (2020)
https://doi.org/10.1063/1.5129650




AIP Publishing

Review of Scientific Instruments ARTICLE scitation.org/journal/rsi

# Design and development of an Allison type emittance scanner for the SPIDER ion source

Cite as: Rev. Sci. Instrum. 91, 013328 (2020); doi: 10.1063/1.5129650
Submitted: 30 September 2019 • Accepted: 7 January 2020 •
Published Online: 24 January 2020



Carlo Poggi,[1,2,a] Emanuele Sartori,[1,2] Marco Tollin,[1] Matteo Brombin,[1] Matteo Zaupa,[1] Enrico Fagotti,[3] and Gianluigi Serianni[1]

## AFFILIATIONS

[1]Consorzio RFX (CNR, ENEA, INFN, Università di Padova, Acciaierie Venete S.p.A.), C. Stati Uniti 4, 35127 Padova, Italy
[2]Università degli Studi di Padova, Via 8 Febbraio 1848, 2, 35122 Padova PD, Italy
[3]INFN-LNL, viale dell'Università 2, 35020 Legnaro (PD), Italy

**Note:** Contributed paper, published as part of the Proceedings of the 18th International Conference on Ion Sources, Lanzhou, China, September 2019.
[a]**Author to whom correspondence should be addressed:** carlo.poggi@igi.cnr.it

## ABSTRACT

Low divergence negative ion beams are crucial for the development of ITER-like fusion reactors. SPIDER is the prototype beam source of the ITER heating neutral beam injector, and it recently started beam acceleration, up to a voltage of 30 kV. The main diagnostics used to measure beamlet divergence are a movable diagnostic calorimeter (STRIKE), which gives the thermal footprint of the beamlets; beam emission spectroscopy; and visible imaging. These systems do not allow a direct measurement of single beamlet phase-space distribution, which is useful for comparison with numerical simulations and to estimate accelerator performances. To this purpose, a movable Allison type emittance scanner for the SPIDER negative ion beam was developed and proposed for the installation on the STRIKE supporting structure. This paper describes the numerical analyses performed to dimension the mechanical and electrical components, such as the Faraday cup and the slits. An analytical approach based on the integration of an arbitrary phase-space distribution was adopted in order to simulate the device performances. The constraints due to the operation in a high heat load environment are discussed.





## I. INTRODUCTION

SPIDER is the prototype ion source of the ITER heating neutral beam.[1] It is designed to accelerate up to 46 A of negative hydrogen extracted from a RF plasma, at a voltage of 100 kV, using a three grid acceleration system. The current is extracted from 1280 beamlets, organized in 16 groups of 80 beamlets each. The expected e-fold divergence for one beamlet at perveance match (i.e., the accelerator perveance for which divergence is minimum) is 5 mrad,[2] and three diagnostics are currently used to assess it:[3] a movable diagnostic calorimeter (STRIKE), which gives the thermal footprint of the beamlets; beam emission spectroscopy; and visible imaging. None of those systems can provide a direct measurement of velocity distribution of the particles belonging to a single beamlet, which would allow us to investigate nonlinear effects in the phase-space distribution of the beamlets and would be useful for comparison with numerical simulations. To this purpose, we propose the installation of a movable Allison type emittance scanner[4] on the STRIKE supporting structure.[5] The device will move vertically using its own motorization, measuring up to half a beamlet group (14 cm) in 1 min. It will also move horizontally and along the beam axis (from 50 cm to 100 cm from the grounded grid) using SPIDER motorization. A sketch of the device is shown in Fig. 1. Currently, SPIDER has only 5 beamlets per group left open, after the introduction of a copper mask in front of the plasma grid to reduce vessel pressure and to reduce the probability of discharges outside the RF source. Acceleration voltage can be applied between 20 kV and 30 kV, and negative ions are generated from volume production, with cesium operation planned for early 2020. A mathematical description of the diagnostic is reported in Sec. II, while Sec. III is devoted to the design of the Allison scanner for SPIDER. Section IV presents the signals expected during operation.

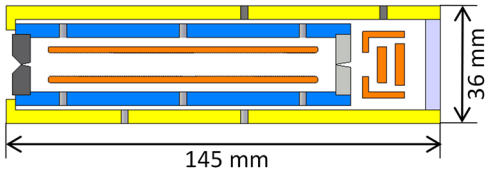


**FIG. 1**. Section view of the emittance scanner, showing slits (gray), plates (orange), Faraday cup (orange), and external shielding (blue and yellow).

## II. MODELING THE EMITTANCE SCANNER

An Allison emittance scanner can be represented by two aligned slits of vertical heights s in the x direction and horizontal widths w in the y direction, and a uniform vertical electric field E in the space region of length D between them. Particles passing through both slits are collected on a Faraday cup. From now on, the frame of reference is centered in the middle of the entrance slit, with the z axis oriented toward the second one.

Considering a non-relativistic beam of particles with velocity $\boldsymbol{v} = (v_x, v_y, v_z)$ and kinetic energy per charge $V_b = \frac{1}{2}\frac{m}{q}v^2 \approx \frac{1}{2}\frac{m}{q}v_z^2$ in a paraxial approximation ($m$ is the mass and $q$ is the charge), the transverse emittance is defined in the 4-dimensional phase space ($x$, $x'$, $y$, $y'$), with $x' = v_x/v_z$ and $y' = v_y/v_z$. The equation of motion of a particle of charge $q$ inside the device in the ($x$, $x'$) plane is $x(z) = x_0 + x_0'z + \frac{E}{4V_b}z^2$, with $x_0 = x(0)$ and $x_0{}' = x'(0)$, and therefore, the conditions on ($x_0$, $x_0{}'$) for a charged particle to pass through both slits are

$$\begin{cases} -s/2 < x_0 < s/2, \\ -s/2 < x_0 + x_0'D + \frac{E}{4V_b}D^2 < s/2, \end{cases} \tag{1}$$

corresponding to four linear inequalities which give the acceptance domain ΩX of the diagnostic for a fixed electric field (similar equations hold for the ΩY domain). The synthetic signal of the device is then obtained by integration of the phase-space distribution $f(x_0, x_0', y_0, y_0')$ of the beam current at the entrance of the diagnostic over the accepted domain,

$$I_{syn} = I_{beam}\int_{\Omega X}\int_{\Omega Y} f(x_0, x_0', y_0, y_0')dy_0dy_0'dx_0dx_0'. \tag{2}$$

The volume of the 4-dimensional acceptance domain $\omega(\Omega X \times \Omega Y) = \omega(\Omega X)\omega(\Omega Y)$ is the acceptance of the diagnostic for a fixed value of electric field and beam energy. The domain defined by (1) in $(x_0, x_0')$ is a parallelogram of fixed area $A = \frac{s^2}{D}$, and this holds for any value of $E$ and $V_b$.[6] However, more parameters need to be included in the model to estimate the acceptance limits of the diagnostic.

### A. Additional parameters and constraints

Real slits have finite size along the $z$ direction. Let this size be $h$. Assuming zero electric field inside the slits, the new equation of motion is

$$\begin{cases} x(z) = x_0 + x_0'z \quad if \quad 0 < z < h, \\ x(z) = x_0 + x_0'z + \frac{E}{4V_b}z^2 \quad if \quad h \leqslant z < D - h, \\ x(z) = x_0 + x_0'(D-h) + \frac{E}{4V_b}(D-2h)^2 + \left(x_0' + \frac{E}{2V_b}(D-2h)\right)z \\ \quad if \quad D - h \leqslant z < D. \end{cases}$$

Thus, a beam particle passes through the first slit if

$$\begin{cases} -s/2 < x_0 < s/2, \\ -s/2 < x(z=h) < s/2 \end{cases} \tag{3}$$

and through the second one if

$$\begin{cases} -s/2 < x(z = L-h) < s/2, \\ -s/2 < x(z = L) < s/2, \end{cases} \tag{4}$$

giving eight linear conditions on $(x_0, x_0')$.

The electric field is generated by polarizing two parallel metallic plates with a voltage difference $V$ between them. These plates are placed perpendicularly to the $x$ direction; let $g$ be the distance between them: the electric field is then $E = -V/g$. A beam particle reaches the Faraday cup if it does not hit the plates at $x = \pm g/2$, that is, if the stationary points of $x(z)$ are between $-g/2$ and $+g/2$. The condition is

$$-\frac{g}{2} < x_0 - \frac{V_b}{E}x_0'^2 < \frac{g}{2}, \tag{5}$$

and it is quadratic in $x_0'$. If $g \gg s$, only one inequality holds, depending on the sign of $E$, and this can be linearized at $x_0 = 0, x_0' = \pm\sqrt{\frac{|V|}{2V_b}}$, obtaining $\frac{x_0}{g} \pm \sqrt{\frac{2V_b}{V}}x_0' < 1$ for $E < 0$ and $\frac{x_0}{g} \pm \sqrt{-\frac{2V_b}{V}}x_0' > -1$ for $E > 0$. The ten constraints in (3)–(5) distort the acceptance domain ΩX, as shown in Fig. 2. Similar conditions are derived for ΩY.

### B. Numerical simulations

Integration domains ΩX, ΩY and their volumes were numerically determined for different design parameters ($s$, $w$, $h$, $D$, $g$, $V$, $V_b$): the intersection of the ten linear conditions described above was determined and triangulated to allow a numerical integration by analytic functions on it. The integral in (2) was calculated with $f(x_0, x_0', y_0, y_0') = \frac{x_0}{\omega(\Omega X)\omega(\Omega Y)}$ to estimate the average value of the $x_0$ coordinate ($\overline{x_0}$) measured by the diagnostic. The error on this value,

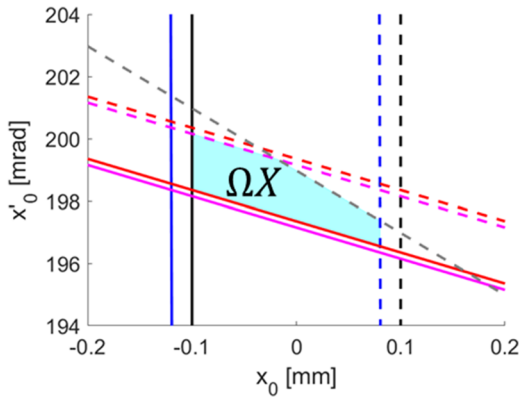


**FIG. 2**. Acceptance domain ΩX identified by conditions (3)–(5). Parameters are $s$ = 0.2 mm, h = 0.1 mm, $D$ = 100 mm, g = 10 mm, $V_b$ = 20 keV, and $E$ = 159 kV/m. Dotted lines correspond to upper limits, and continuous ones correspond to lower. Black and blue lines stand for conditions (3), red and magenta for (4), and gray line for (5). The shadowed region is no longer a parallelogram.

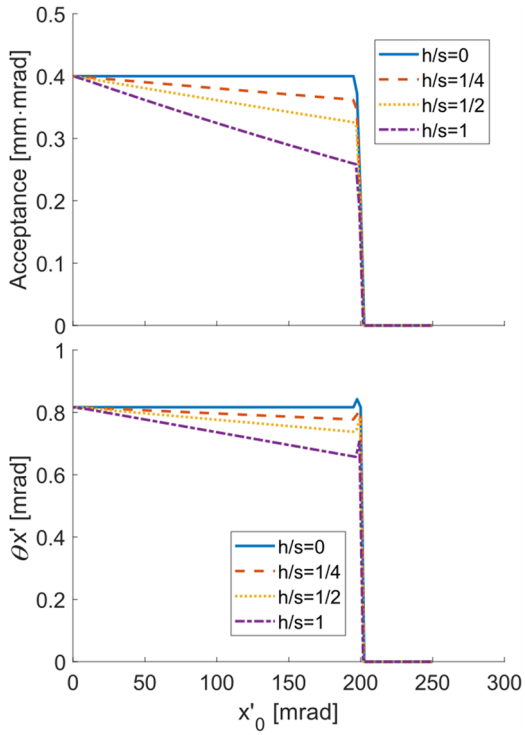


**FIG. 3**. Acceptance and angular error of the diagnostic for different h. Diagnostic parameters are $s$ = 0.2 mm, $D$ = 100 mm, g = 10 mm, and $V_b$ = 20 keV; E is varied in the range $-2 \times 10^5$ V/m to $2 \times 10^5$ V/m.

$\theta_{x0}$, was calculated by taking the square root of the integral in (2) calculated with $f(x_0, x_0', y_0, y_0') = \frac{(x_0 - \overline{x_0})^2}{\omega(\Omega X)\omega(\Omega Y)}$. The same calculations were performed also for $x_0'$, whose average value is given by

$$\overline{x_0'} = \frac{V(D-2h)}{4gV_b}. \tag{6}$$

Figure 3 presents the acceptance and angular error of the diagnostic ($s$ = 0.2 mm, D = 100 mm, g = 10 mm, $V_b$ = 20 keV) as a function of the average angular coordinate $\overline{x_0'}$ for various values of $h$. The limit calculations reproduce the values predicted by Allison with the ideal model (h/s = 0 case, corresponding to an acceptance of $A = \frac{s^2}{D}$ = 0.4 mm mrad and an error of $\sigma_{x'} = \frac{s}{\sqrt{6}D}$ = 0.82 mrad) but show a variation with increasing $|x_0'|$, and the absolute value of the slopes increases linearly with the ratio $h/s$.

## III. DESIGN OF THE SCANNER AND APPLICATION TO SPIDER BEAM

Currently SPIDER operates with single beamlets having divergence between 20 mrad and 30 mrad at 20–30 keV, transporting 1.5 mA of current each. To have a good measurement range, the scanner must then accept entrance angles up to 100 mrad. The limitation due to $g$ gives $x'_{MAX} = 2g/D$, which for $D$ = 100 mm yields $g > 5$ mm. We have chosen $g$ = 8 mm, which accepts up to 160 mrad. From Eq. (6), the voltage needed at 30 keV to deflect particles with $x_0'$ = 100 mrad is at least $V_{MIN} \geq \frac{4g}{D} V_b x_0'$ = 0.96 kV. The beamlet footprint on STRIKE is approximately 4 cm wide, with a horizontal displacement of about 1 cm from one row to the next one. Thus, a horizontal slit dimension $w$ = 80 mm was chosen, allowing a complete integration of two subsequent beamlets in the $y$ direction with a vertical scan. The slit vertical dimension $s$, which determines the angular resolution of the device, was chosen by imposing that the minimum collected current at the Faraday cup is 100 nA for angles twice as much as the e-fold divergence. From this condition, we determined s = 0.4 mm (corresponding to $\sigma_{x'}$ = 1.6 mrad) for current volume operation (3 mA beamlet of 20 mrad divergence) and s = 0.2 mm ($\sigma_{x'}$ = 0.8 mrad) for future cesium operations (19 mA at 5 mrad divergence). Assuming mechanical tolerances to be 50 $\mu$m, the $h/s$ ratio is expected to be 1/4 at most, thus giving a 2.4% reduction of device acceptance at 50 mrad.

### A. Fringe field effects

The metallic plates are placed at a distance of 10 mm from the slits (6 mm from the slit walls) and present a sawtooth pattern 0.2 mm deep and with 20° angle to suppress ghost signals.[7] The minimum geometric distance between the plates is then 7.6 mm. Electrostatic simulations were made with COMSOL code[8] to assess the effect of fringe fields. Plots of the $x$ component of the electric field generated by a 1 kV voltage difference along paths parallel to $z$ at different $x$ are shown in Fig. 4. The average intensity of the electric field between the plates ($z > 15$ mm) is $E_0$ = 130 kV/m, corresponding to $g_{eff}$ = 7.7 mm. The sawtooth pattern produces oscillations around this value, which are below 1% up to $x$ = 3.5 mm, thus reducing the maximum accepted distance between the plates to 7 mm.

The finite size of the metallic plates produces a non-zero electric field in the region before the plates, with a peak at $z$ = 9.6 mm for $x > 3$ mm. To avoid its effect, the slits present a hollow on the face oriented toward the plates, which forces the particles to reach $z$ = 10 mm at a maximum height of 2 mm. The non-zero electric field before the plates is considered in the model by replacing the distance $D$ between the slits with the effective distance[9]

$$D_{eff} = \int_0^{3.5\text{ mm}} \int_0^{D} \frac{E_x(x,0,z)}{3.5\text{ mm} \cdot E_0} dz dy = 93.6 \pm 0.4 \text{ mm}.$$

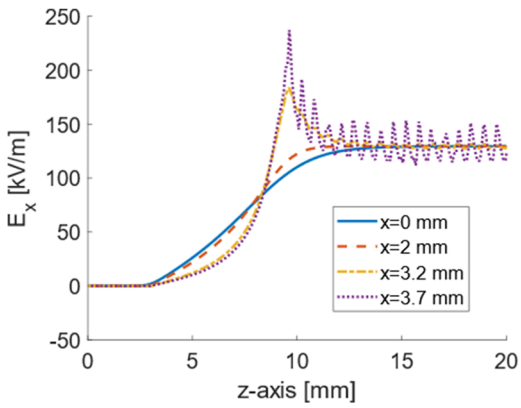


**FIG. 4**. Plot of $E_x$ along the z axis at various x coordinates.

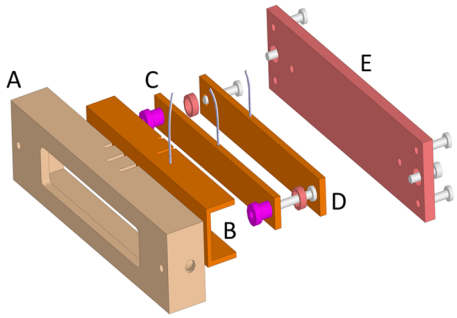


**FIG. 5**. Exploded view of the Faraday cup, showing PEEK insulators (A and E), copper electrodes (repeller B, collector C, and reference D), ceramic bushings, and screws.

### B. Faraday cup

An exploded view of the Faraday cup is presented in Fig. 5, showing the suppressor, the collector, and the reference electrodes, together with the insulating parts. Simulations of the secondary electron emission from copper due to impinging hydrogen ions were performed with OPERA code[10] to assess Faraday cup performances. The secondary electron yield was assumed to be 1.5, with an exit energy of 50 eV. These conditions are worse than real cases modeled in the literature.[11] Under those assumptions, a voltage difference of 200 V was found sufficient to collect all secondary electrons.

### C. Thermal simulations

Supporting parts of the device exposed to the SPIDER beam will be covered with graphite tiles, and only an area of 7 mm × 80 mm of the pieces composing the front slit (which will be made of molybdenum) will be exposed to the accelerated particles. Furthermore, those pieces will present a 45° angle in order to decrease the heat load. Ansys simulations were performed to verify the thermal limits of the designed scanner. The present SPIDER operation with isolated beamlets and without cesium was found not demanding for the device due to the small current and high divergence. Therefore, only cesium operating regimes were analyzed for both isolated and multi-beamlet configurations. Time domain simulations were performed assuming the beamlets are centered on the device first slit and deposit power for 1 min and are then turned off for 9 min (10% duty cycle). Beamlet divergence was always assumed to be optimal (5 mrad), and current was obtained from perveance match. Results for different voltages and distances of the detector are shown in Fig. 6.

Apart from 100 kV acceleration voltage cases, other conditions shown are acceptable: the isolated beamlet configuration [Figs. 6(a) and 6(b)] shows a peak of 400 °C for the 50 kV case (which corresponds to 70% of the nominal current) with the detector at 50 cm from the source, and temperature goes back to starting values after one cycle. As for the multi-beamlet configuration [Figs. 6(c) and 6(d)], peak temperature is around 800 °C after 1 min, which is still acceptable, but does not decrease to starting values after one cycle. This can be obtained by reducing the duty cycle to 5%.

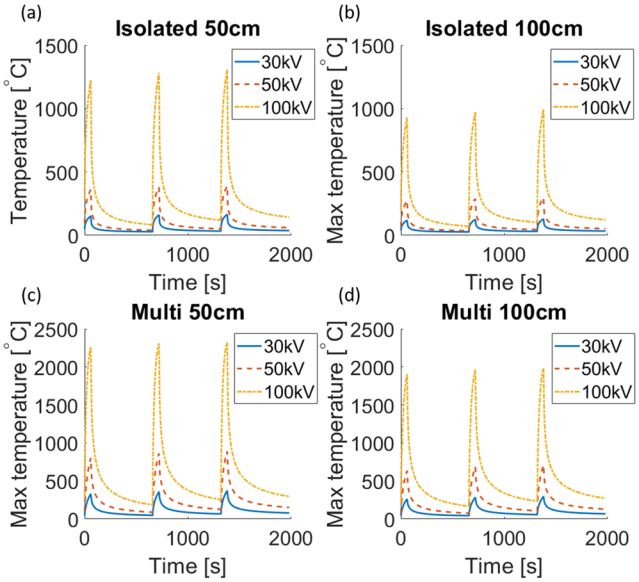


**FIG. 6**. Maximum temperature of the device for the isolated beamlet configuration (a) at 50 cm and (b) at 100 cm. Maximum temperature of the device for multi-beamlet configuration (c) at 50 cm and (d) at 100 cm.

## IV. APPLICATION TO THE SPIDER BEAM

The diagnostic will operate in a relatively high-pressure environment (SPIDER vessel pressure is between 0.02 mPa and 0.05 mPa), and therefore, the interaction of the beam with background gas can become relevant. These interactions can produce other kinds of fast species, such as $H^+$ and $H^0$, which as a first approximation would have the same phase-space distribution as the original $H^-$ beam. Figure 7 presents the fractions of fast species at different distances from the last accelerator grid, for a vessel pressure of 0.05 Pa and a beam energy of 20 keV. Cross sections

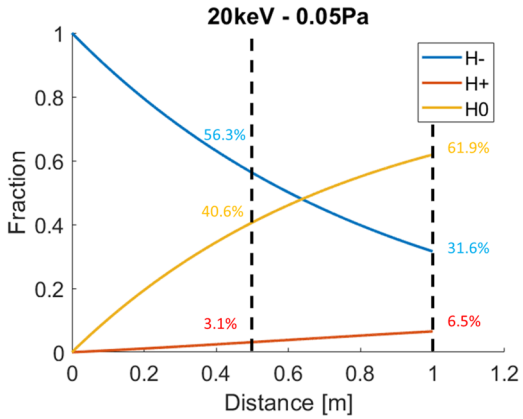


**FIG. 7**. Fractions of fast species present at different distances from the SPIDER grounded grid, starting from an $H^-$ beam. Black dashed lines show minimum and maximum scanner positions, and fractions at those positions are also reported.

considered are stripping and double stripping of $H^-$, ionization of $H^0$, and neutralization of $H^+$, with data taken from Ref. 12.

The emittance scanner is not able to distinguish between positively and negatively charged particles with opposite entrance angles. Therefore, two overlapping beams of opposite charge will be collected by the Faraday cup but traveling at opposite angles. The measured current at the Faraday cup for certain position and angle will then be

$$I_{FC}(x_0, x_0') = I_{H-}^{acc}\left(f_{H-}(x_0, x_0') - f_{H+}(x_0, -x_0')\right), \quad (7)$$

where $I_{H-}^{acc}$ is the $H^-$ current at the accelerator exit and $f_{H-}$ and $f_{H+}$ are the particle fractions at detector position (we are assuming $H^-$ current to be positive). OPERA simulations were used as estimation of single beamlet phase-space distribution. The total number of simulated rays is of the order of $10^3$. Since we are interested in phase-space distribution, it was necessary to increase the number of particles to have a good sampling of the phase-space domain. In order to do so, for each of 4 transverse dimensions, an average distance between particles was defined as

$$d_p = \frac{1}{2N(N-1)} \sum_{i=1}^{N-1} \sum_{j>i}^{N} |p_i - p_j|, \quad (8)$$

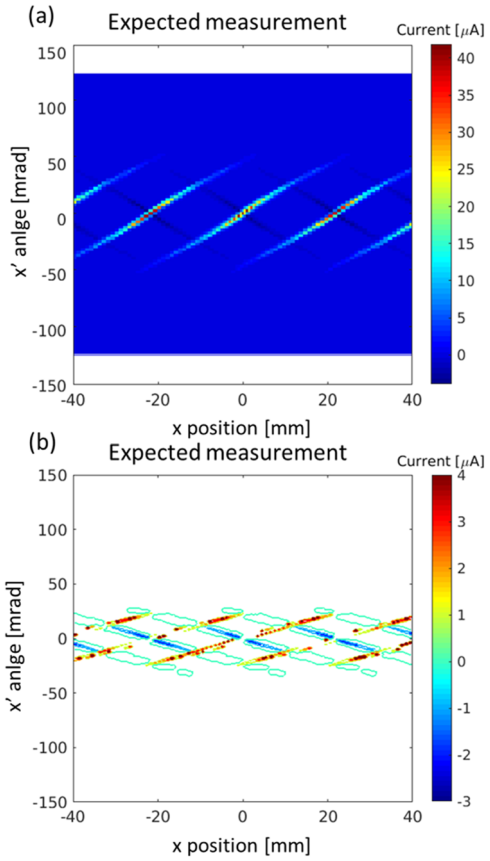


**FIG. 8.** (a) Expected signal at the Faraday cup assuming 50 mPa vessel pressure: positive ion distribution is slightly visible. (b) Contour plot of the signal up to 10% of maximum value to highlight the contribution of the positive ion.

where N is the total number of simulated particles and $p_{i,j}$ is any of the transverse variables x, x′, y, and y′. For each of the N particles, $2.4 \times 10^7$ random particles were generated with a uniform distribution in the 4-D hypercube of dimensions ($\alpha dx$, $\alpha dx'$, $\alpha dy$, $\alpha dy'$), with $\alpha = 0.2$. Each particle was then transported at detector position, assuming complete space charge compensation, and the AES signal was estimated by integrating the distribution given by Eq. (7) on $\Omega X$ and $\Omega Y$ calculated for various voltages applied between the plates. We report in Fig. 8 an example of this calculation, for a multi-beamlet configuration obtained by constructing a 5 × 5 beamlet matrix in $x$ and $y$ positions, starting from a 20 kV, 16 A/m$^2$ single beamlet and measuring in $x$ and $x_0'$ after integration in $y$ and $y'$. Figure 8(a) shows the expected signal assuming a vessel pressure of 50 mPa: tails of beamlet distributions are visible, and it is also possible to notice the effect of the positive ion beam, which is better highlighted in Fig. 8(b).

## V. CONCLUSIONS

An Allison emittance scanner was developed for use in the SPIDER ion source. The diagnostic was designed to work under current operating conditions of SPIDER, with a configuration featuring isolated beamlets. Thermal analysis showed that it can operate in both volume and cesium operation up to an acceleration voltage of 50 kV with a 10% duty cycle and in multi-beamlet configuration by reducing the duty cycle to 5%. Signal estimation starting from beam optics simulations showed that the device can be used to study the tails of beamlet phase-space distribution and can also detect positive ions generated by beam-gas interaction.

## ACKNOWLEDGMENTS

The work leading to this publication had been funded partially by Fusion for Energy (F4E). This publication reflects the views only of the authors, and F4E cannot be held responsible for any use which may be made of the information contained therein. The views and opinions expressed herein do not necessarily reflect those of the ITER organization. The authors have confirmed that any identifiable participants in this study have given their consent for publication.

## REFERENCES

[1] G. Serianni, V. Toigo, M. Bigi, M. Boldrin, G. Chitarin, S. Dal Bello, L. Grando, A. Luchetta, D. Marcuzzi, R. Pasqualotto *et al.*, Fusion Eng. Des. **146**(B), 2539–2546 (2019).
[2] P. Agostinetti, D. Aprile, V. Antoni, M. Cavenago, G. Chitarin, H. P. L. de Esch, A. De Lorenzi, N. Fonnesu, G. Gambetta, and R. S. Hemsworth, Nucl. Fusion **56**, 016015 (2016).
[3] R. Pasqualotto, M. Agostini, M. Barbisan, M. Brombin, R. Cavazzana, G. Croci, M. Dalla Palma, R. S. Delogu, M. De Muri, A. Muraro *et al.*, J. Instrum. **12**, C10009 (2017).
[4] P. W. Allison, J. D. Sherman, and D. B. Holtkamp, IEEE Trans. Nucl. Sci. **30**, 2204–2206 (1983).
[5] E. Sartori, M. Zaupa, G. Serianni, and R. Pasqualotto, Plasma Fusion Res. **13**, 3405092 (2018).
[6] R. D'Arcy and A. Shemyakin, "Calculation of the effect of slit size on emittance measurements made by a two-slit scanner," arXiv:1503.06055 [physics.acc-ph].
[7] M. P. Stockli, M. Leitner, D. P. Moehs, R. Keller, and R. F. Welton, AIP Conf. Proc. **763**, 145 (2005).

[8]COMSOL Multiphysics® v. 5.3, COMSOL AB, Stockholm, Sweden, 2017, www.comsol.com.
[9]H. Wollnik and H. Ewald, Nucl. Instrum. Methods **36**, 93–104 (1965).
[10]G. Fubiani, H. P. L. de Esch, A. Simonin, and R. S. Hemsworth, Phys. Rev. Spec. Top.–Accel. Beams **11**, 014202 (2008).
[11]OPERA 3d, Cobham Technical Services, Vector Fields Software, Oxford, UK.
[12]C. Barnett, NASA STI/Recon Technical Report N 91, 1990.